http://eprints.gla.ac.uk/149720/

Deposited on: 16 November 2017

High Performance CuO Nanorectangles based Room Temperature Flexible NH₃ Sensor

Bhuvaneshwari Sakthivel, Libu Manjakkal, Gopalakrishnan Nammalvar

Abstract— **Here, we report the fabrication of a flexible room temperature ammonia gas sensor using surfactant-free hydrothermally synthesized copper oxide (CuO) nanorectangles. The structural analysis revealed that the CuO nanorectangles possessed monoclinic structure with an average length and breadth of 950 nm and 450 nm respectively. The specific surface area of CuO nanorectangles was determined to be 29 m²/g. The sensor was fabricated on a flexible polyethylene terephthalate substrate by screen printing technique. The room temperature ammonia sensing measurement exhibited significant response down to 5 ppm of ammonia with a quick response time of 90 s and recovered to baseline within 120 s. Maximum response of 0.99 was recorded for 100 ppm of ammonia. The rate constants for adsorption and desorption were estimated for 6.5 to 100 ppm of ammonia from the exponential conductance changes during response and recovery process. The sensor showed appreciable stability and reproducibility of the sensing performance over a period of 3 months. The fabricated flexible sensor demonstrated its ability to detect a wide range of ammonia concentrations at room temperature irrespective of the mechanical deformations applied. Thus, the fabricated sensor is promising and can be suitably employed for practical applications in environments where efficient gas sensing is vitally important.**

Index Terms—**CuO, Nanorectangles, Flexible gas sensor, Screen printing, Rate constants.**

I. INTRODUCTION

Toxic gases such as ammonia (NH₃), carbon monoxide (CO), hydrogen sulphide (H₂S), etc. from industrial exhausts or wastes cause long term health issues [1, 2] and could have grave impact on the quality of life of the workers. The continuous observation of these gases will allow monitoring the health of workers. The development of NH₃ various gas sensors has reported by several researchers, and ammonia is one of the gases taken seriously due to its natural and industrial origin [3-5].

Dr. Bhuavaneshwari Sakthivel and Dr. Gopalakrishnan Nammalvar are with National Institute of Technology, Tiruchirappalli, India. (e-mail: bhuvana.psv@gmail.com and ngk@nitt.edu)
Dr. Libu Manjakkal is with University of Glasgow, U.K and Institute of Electron Technology, Krakow Division, 30-701 Krakow, Zablocie 39, Poland (Libu.Manjakkal@glasgow.ac.uk)

However, low level detection of NH₃ is still requires robust and inexpensive systems for real-time monitoring at ppb-ppm levels in environmental monitoring, food processing and medical applications.

In this regard, wearable electronics, which has gained significant attention recently, opens a new window possibly enabling self-health management. For better integration with wearable systems, sensors should be flexible, small in size, and portable. Flexible sensors based on metal oxide (MOₓ) nanostructures have attracted significant attention considering their high sensitivity, low production cost, ease of fabrication, wear-ability and eco-friendliness [9, 10]. There have been several reports on MOₓ based sensors such as SnO₂, ZnO, TiO₂, WO₃, InO₃, CuO, Co₃O₄ and NiO due to their extremely high sensitivity to hazardous gases (for instance H₂S) as well as better selectivity to certain volatile organic compounds (VOCs) [11-19]. The adsorption induced variation in electrical resistance of MOₓ based gas sensors have been used for the detection of gases such as NH₃ in ppb (parts-per-billion) range [6]. The features such as long-term stability and low-power consumption have been recently demonstrated in nanostructures (nanorods, nanosheets, and urchin-like) based metal oxide gas sensors for the detection of NH₃, CO, H₂S, etc. [6-8]. However, these reported sensors require undesirably high operating temperatures to yield stable response whereas for wearable applications, ambient temperature operation of gas sensors is desirable.

Copper oxide (CuO) is a well-known *p*-type, thermo-stable MOx semiconductor with a narrow band gap of 1.4 eV and has been widely used as catalytic and adsorption material [19]. CuO with different morphologies such as nanowires, nanorods, nanoribbons, etc. structures have been utilized for sensing different gases [20-23]. The unique properties and sensing mechanism of CuO nanostructures have exhibited promising gas sensing properties towards various gases such as ethanol, methanol, other volatile organic compounds (VOCs) and other toxic gases [23]. Few reports have shown the long-term stability and low power consumption by fabricating gas sensors using CuO nanorods, nanowhiskers, nanoflowers, urchin-like towards for target gases like NH₃, CO, H₂S etc. However, most of the sensors needed higher operating temperature as mentioned above to show stable response. Moreover, only few sensor parameters were explored.

This work presents the development of CuO based flexible gas sensors for NH₃ detection at room temperature. Single phase CuO nanorectangles (NRs) were synthesized by a simple hydrothermal route and characterized for various

physio-chemical properties. The sensor was fabricated using screen printing, which is a well-established cost-effective technique for the fabrication of sensor systems on flexible and other different types of substrates [24, 25]. The fabricated sensors are operable at room temperature and exhibited superior response as compared to similar type of sensors reported in literatures. The flexible CuO sensor capable of sensing NH₃ of concentrations as low as 5 ppm. In this work, the detailed kinetics of sensing response is analyzed using non-linear regression models and the relationship between time constants and sensor response is also established. Apart from this, stability experiments were performed on the sensor which revealed the high reproducibility of sensing performance towards various concentrations of NH₃.

II. MATERIALS AND METHODS

A. Synthesis of CuO nanostructures

CuO nanostructures were synthesized by mixing 0.1 M of Copper nitrate hemi pentahydrate (Alfa aesar, 98 % purity) and 0.7 M of NaOH (Alfa aesar, 98 % purity) in 75 ml de-ionized water under vigorous stirring for 60 min at room temperature. The dark blue solution obtained following these steps was transferred to a Teflon lined autoclave and kept in the furnace for 12 h at 160°C. The obtained precipitate was washed by centrifugation with water and ethanol several times and dried in air for 24 h.

B. Flexible CuO sensor device fabrication

Initially, the CuO sensitive layer was prepared by mixing the synthesized CuO nanopowder with 50 wt.% of copolymer which comprised of PMMA-PMBA [Poly (methyl methacrylate)-poly (butyl methacrylate)] as binder and BCA [butyl carbitol acetate (ZCHO, Poland)] as solvent in an agate mortar for 1 hour. The screen for interdigited electrode (IDE) was prepared with the following dimensions: finger lengths of 10 mm, electrode width of 0.5 mm and spacing between fingers of 0.5 mm. Fig.1a shows the screen-printed IDE using silver (Ag) paste (DuPont 5000) on PET substrate (Fig.1b). After printing, the electrode layer was dried at 120 °C for 20 min. Further, the CuO sensing element with an area of 1×1
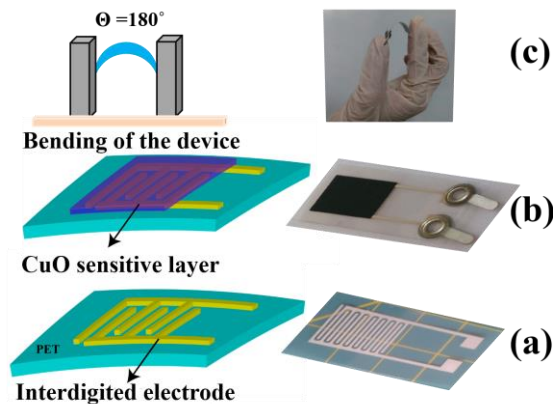

Fig.1. (a) Schematic and digital images of the fabricated sensors and (b) & (c) shows the bending condition enforced and the flexibility of the fabricated device.

cm² was printed on the top of the IDE layer as shown in Fig.1b. The fabricated CuO layer then dried at 120 °C for 2 hours. The bending condition and the flexibility of the device is shown Fig.1c.

C. Gas sensing measurements

The NH₃ sensing efficiency of the device at room temperature was examined in an indigenous gas sensing setup [7]. In brief, static state distribution method was followed for the sensing measurement as follows. Initially, the stable data collection was ensured by preheating the sensor device inside the test chamber to overcome the storage related reversible resistance drift. Further, a predetermined volume of NH₃ was introduced in the sensing chamber. The required concentration of NH₃ vapor was calculated using the following equation [26];

$$C_{ppm} = \frac{V_{\mu L} D_{g/mL}}{M_{g/mol} V_{mL}} \times 2.24 \times 10^7 \qquad (1)$$

where, C_{ppm} is the required vapor concentration, $V_{\mu L}$ is the volume of liquid analyte, $D_{g/mL}$ is the density of the liquid, V_{mL} is the volume of test chamber and $M_{g/mol}$ is the molecular weight of the liquid analyte (all the subscripts are the respective units). Sensing studies were carried out using the commercially available NH₃ (99 % purity) at room temperature and under ambient conditions (temperature – 27 °C and laboratory relative humidity (RH) 55 - 70 %). A constant voltage of 3V was applied to the sensor and the relative change in sensor resistance was monitored and recorded as sensing signal. Prior to introduction of NH₃ every time, the baseline resistance was measured. The sensing response is calculated from the relative change in sensor's electrical resistance under NH₃ environment by the following equation [26],

$$S = \frac{R_G - R_a}{R_a} \qquad (2)$$

where, R_a is sensor resistance in air ambience, and R_G is the resistance in NH₃ atmosphere.

D. Characterization techniques

The crystal structure and phase analysis of the sample (powder and film) were carried out using X-ray diffractometer [Rigaku Ultima III, with Cu K$_\alpha$ (λ=1.514 Å) radiation]. Spectrum RX-FT-IR spectrometer (Perkin Elmer, USA) was utilized for vibration spectroscopy and functional group analysis. The 514.5 nm line from a Renishaw Micro Raman spectrometer with 5 mW argon ion laser as excitation source was used to confirm the structural properties of the CuO nanopowder and the sensor device. Morphological and elemental analyses were performed in a Zeiss ULTRA 55 field emission scanning electron microscopy (FESEM). Transmission Electron Microscopy (TEM) analysis was carried using a Philips CM 200 microscope. The surface morphology and roughness of the film were investigated in non-contact mode by Atomic Force Microscopy (AFM) (Park System's NX-10, South Korea) with a silicon nitride cantilever. For AFM analysis, a scan size of 10 μm and scan rate of 0.5 Hz was used. Surface area and porosity measurements were carried out at liquid nitrogen temperature using a Quantachrome Nova-1000 surface analyzer. N₂ adsorption–desorption isotherm cycle measurements were

performed up to the saturation vapor pressure of nitrogen (−196 °C) and the pore size distribution was determined from the adsorption data using BJH and de Boer's t-method.

III. RESULTS AND DISCUSSIONS

A. Structural analyses of CuO powder and film

The XRD patterns (Fig.2a) of the samples is indexed according to the monoclinic structure (JCPDS data 45-0937) of CuO and there is no evidence of any impurity phases in XRD spectra of both as-prepared powder and fabricated sensor. The lattice parameters (a ≠ b ≠ c and α = γ = 90 ° ≠ β for monoclinic structure) were evaluated from the following equations (3) and (4);

$$n\lambda = 2d\sin\theta \tag{3}$$

$$\frac{1}{d^2} = \frac{1}{Sin^2\beta}\left(\frac{h^2}{a^2} + \frac{\sin^2\beta}{b^2} + \frac{l^2}{c^2} - 2hl\cos\frac{\beta}{ac}\right) \tag{4}$$

The obtained values are a= 4.688 Å, b= 3.427 Å, c= 5.132 Å, for CuO powder and a = 4.688 Å, b= 3.427 Å, c= 5.132 Å for CuO based sensor device. The average crystallite size of 35 nm was estimated using the standard Scherrer's relation $D = k\lambda/\beta\cos\theta$, where D is the crystallite size, k the shape factor, β is the fullwidth half maximum. It is clear that there is no change in crystal structure observed for the film. The calculated lattice parameters found to closely match with those reported in literatures [3, 27].

The FTIR spectra recorded in the range 400 to 4000 cm^{-1} for the CuO powder and CuO thick film is shown in Fig. 2b. The three signature peaks observed at 418, 496 and 603 cm^{-1} belongs to the Au, Bu and the other Bu modes of CuO. The high frequency peak at 603 cm^{-1} can be attributed to the Cu-O stretching along the (-101) direction. Absence of any peaks in the 605-660 cm^{-1} range rules out the existence of Cu$_2$O phase. The broad absorption at 3394 cm^{-1} can be attributed to the stretching vibration of absorbed H$_2$O or surface hydroxyls of the sample, and the bands at 1553 and 1378 cm^{-1} are assigned to the asymmetrical stretching vibration and symmetrical stretching vibration of RCOO$^-$ absorbed on the surface of CuO, respectively. It is evident that there is no presence of vibrational modes related to the binder molecules on the surface of CuO film observed indicates the purity of the device. Fig.2c shows the micro-Raman spectra recorded for the CuO nanopowder and film. The monoclinic phase of CuO belongs to the C$^6_{2h}$ space group, for which the primitive cell contains two molecular units. Thus, from the

selection rule, it is clear that there are twelve vibrational modes at the zone center, including three acoustic modes (A$_u$+2B$_u$), six IR active modes (3A$_u$+3B$_u$) and three Raman active modes (A$_g$+2B$_g$) [27]. Based on group theory, these lattice vibrations at the Γ point of the Brillioun zone are given as,

$$\Gamma = 4Au + 5Bu + Ag + 2Bg \tag{5}$$

From Fig.2c, it is seen that the peaks are broadened and downshifted as compared to the CuO single crystal vibrations [8]. The spectrum shows three peaks at 271, 320 and 596 cm^{-1}. The A$_g$ mode observed at 271 cm^{-1} is associated with the in-phase/out-phase rotations of the CuO asymmetric stretching mode whereas while B$_{1g}$ bending mode existing at 320 cm^{-1}. The B$_{2g}$ mode observed at 596 cm^{-1} is associated with the symmetric oxygen stretching. The three active Raman modes identified here are in accordance with the literature reports [27]. These significant peaks also indicate the single phase and good crystallinity of the as-synthesized CuO nanostructures. The broadening of the peaks can be attributed mainly to the quantum confinement effect of CuO nanostructures [28]. In the case of fabricated film only the three vibrational modes corresponding to CuO nanoparticles are present which rules out the possibility of impurities or binder left over.

B. Morphological and surface analyses of CuO powder and film

Fig.3a shows the FE-SEM image of synthesized CuO nanostructures which illustrates the rectangle-like morphology with smooth surfaces. The thin nature of the NRs with an average thickness of 45 nm can be seen from the TEM image represented in Fig 3b. The NRs are well shaped, blunt edged and are quite transparent. From TEM analysis, the average length is found as 950 nm and while breadth as 450 nm. Fig.3c shows the 2D AFM image of the CuO film. The 5 × 5 µm scan of the AFM image reveals that the CuO sensing layer composed of near uniform distributed nanostructures and void areas. The root mean square surface roughness of the film was found as 130 nm. The statistical analysis revealed the height profile of the film as shown in Fig.3d.

BET surface area analysis was performed on the samples to find examine the adsorption and desorption properties. The N$_2$ adsorption and desorption curves shown in Fig. 3e indicates the type III isotherm behavior due to multilayer adsorption with a narrow H3 type hysteresis loop
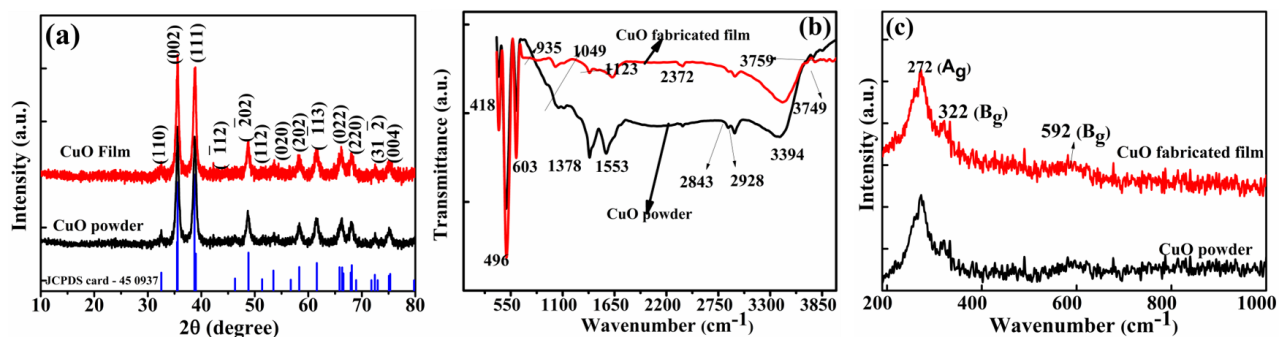

Fig. 2. (a) XRD spectra, (b) FTIR spectra and (c) micro Raman spectra of CuO powder and screen printed CuO film.

between 0.8 to 1 P/P$_0$. The specific surface area of 29 m^2/g was estimated from the adsorption/desorption isotherm. In addition, pore size distribution was calculated from the adsorption data using BJH and de Boer's method (inset in Fig.3e). The characteristic N$_2$ adsorption and desorption isotherms and pore size distribution analyses reveal that the sample is mesoporous (> 2 nm) with average pore diameter of

8 nm. It is important to mention that there is no visible pore structure observed from the morphological analysis. This indicates that the estimated pore size may be from the slit-like pores raised during the assembly of rectangle -like structures. The porosity of the nanomaterial is known to have strong influence on the sensing performance [29].
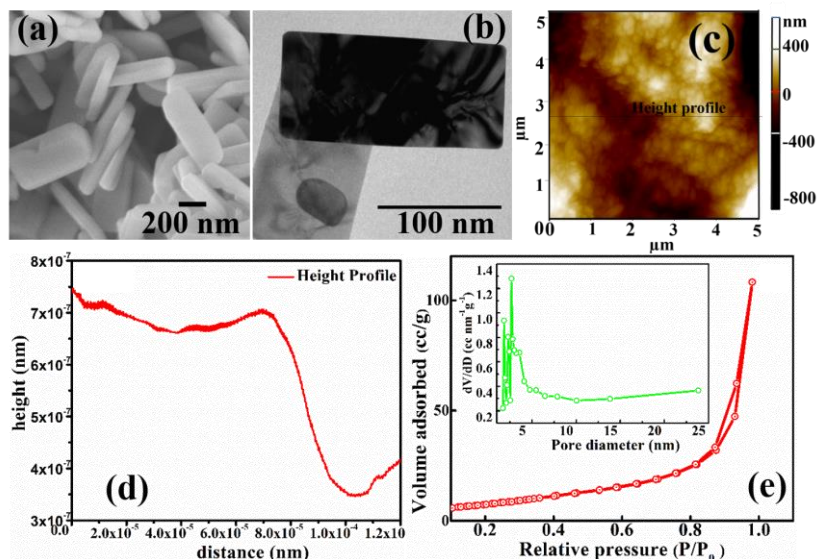

Fig.3: (a) FE-SEM (b) TEM images of CuO NRs (c) AFM image (d) height profile of the CuO film and (e) N$_2$ adsorption - desorption curves of CuO NRs (the inset shows pore size distribution calculated from de-Boer's method).

C. NH$_3$ sensing performance of the flexible CuO sensor

Before being exposed to NH$_3$, the ohmic nature of the fabricated CuO NRs electrode was checked. Fig.4 shows the I-V plot of the sensor device. The output current measurements were made with voltage sweeping between -10 V and +10 V. The linear I-V characteristics of the device shows the good ohmic contacts with no interfacial barrier or traps between the CuO sensing layer and Ag (IDE) electrodes. To check the effect of bending on the electrical properties, the sensor was bent at an angle 90° and kept in this condition for 24 h. The sensor was then brought back to flat condition (this mode of measurement will be mentioned as "after bending") and I-V measurement was carried out. It is seen that the sensor showed I-V characteristics similar to the one before bending it. The average resistance could be calculated from the slope of these lines. The initialization of the sensing response measurement

When the predetermined concentration of NH$_3$ is allowed into the chamber, NH$_3$ molecules interact with the adsorbed oxygen on the surface of CuO sensor, and releases electrons thereby increasing the sensor's resistance. Afterwards, the original base resistance can be retrieved back to the baseline by removing the NH$_3$ supply, and the time taken to bring back the resistance within 10 % of the baseline is known as the recovery time. The sensing performance of the sensor was studied

Fig.5. Sensing performance of flexible CuO sensor before and after bending for different concentrations of NH$_3$ at RT and dotted lines are the corresponding fit (Inset- response of sensors @ RH=50 %).
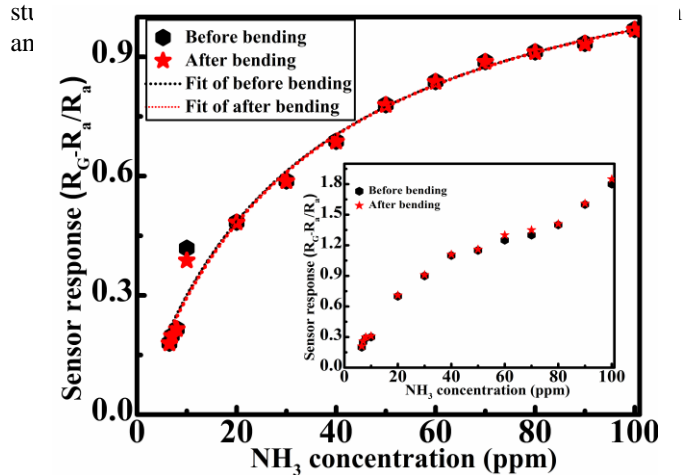

Fig. 4. I-V Characteristics of nanostructured flexible CuO film.

The sensor response is found to increase with increasing NH_3 concentration which is a typical behavior of MO_x sensors [26]. In order to observe the effect of bending on the sensor response, the sensor response was measured after recovering the sensor from bending as mentioned earlier. It is seen that the sensor response is not affected even after a day-long bending and the estimated response is shown in Fig.5. It should be noted that the sensor shows good response down to 5 ppm of NH_3. It is worth mentioning that for automotive industries, the meaningful concentration is from 25 mg/s to 8 ppm [30] and long term allowed concentration is 20 ppm in passenger cabinets [31] for which our sensor showed impressive response of 0.18, 0.20, 0.22 and 0.52 for 5, 7, 8 ppm and 20 ppm, respectively. A maximum response of 0.98 observed for 100 ppm NH_3.

The gas sensing mechanism is a process between the adsorbed species and the MOxs surface [19,26,27]. Upon exposure to air, the atmospheric oxygen is physisorbed on the sensor's surface which is typically temperature dependent. In the case of SnO_2, it was found that the adsorption of O_2 takes place at the sensor's surface at low temperatures [32]. Here, the sensing experiments were carried out in RH $\geq$ 50 % which is comparable to the sensor's environmental conditions for real time applications. Hence, in addition to the physisorbed oxygen, the capillary condensation of water vapor in the adsorption sites of the sensor's surface as per the Grotthus mechanism [33] will be also taken into the account. By considering these two factors, the sensing response of the present sensor was carried out in RH of 50 % and the results are given in inset of Fig.5. It is seen that the sensor response to NH_3 at low concentrations from 5 to 10 ppm is greater by 0.8 % and from 10 – 100 ppm it is greater by 2 %. In addition, the response at RH=50 % found to move towards attaining a linear relationship with the NH_3 concentration. The lower humidity level favors more adsorption of NH_3 while higher humidity level leads a competition of NH_3 and physisorbed oxygen along with water vapor present in the atmosphere. The most probable interaction between the physisiorbed oxygen and water vapor is explained for SnO_2. In the view of this, the present sensing mechanism is explained by the following reactions,

$$O_2 + 2e^- \longleftrightarrow 2O_{ad}^- \qquad (6)$$

$$O_{ad}^- + H_2O + 2Cu + h^+ \leftrightarrow 2(Cu^+ - OH^-) + S \qquad (7)$$
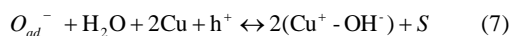
The reaction eqn. 6 shows the adsorption of oxygen molecule on the surface while eqn.7 shows the subsequent reaction with the water vapor in the case of humid atmosphere. This interaction implies that under these adsorption/desorption conditions at high humid conditions, there will be a competition between water vapor and NH_3 for oxygen. Hence, the lesser sensor response observed at laboratory RH compared to 50 % RH. At high humid atmosphere, the formation of dipoles in eqn. 7 hinders the escape of electrons by increasing the work function of the MOx [34]. This mechanism however, further requires prove from direct spectral evidences similar to the reports available for SnO_2 [32, 35]. The observed ultra-high response for such low concentrations of NH_3 can also be attributed to the more adsorption sites facilitated by the high surface area (29 m^2/g) of CuO NRs.

Chemi-resistive sensors rely on the change in resistance mechanism due to the adsorption and desorption of the detected matter. Hence, the change in resistance should be proportional to the amount of the adsorbed and desorbed species onto the surface. The sensing mechanism can be explained in terms of the depletion layer model, using the adsorption-desorption (A-D) kinetics that take place at the crystalline interface and causing the change in carrier concentration. In such a case, the operating temperature, morphology, porosity play a major role along with the concentration and nature of the target gas. The observed response behaviors of Fig. 5 were analyzed with non-linear regression model corresponds to Langmuir adsorption isotherm as follows (dotted lines in Fig. 5) [36, 37],

$$\frac{\Delta R}{R_0} = \frac{Q_{sat} \times k \times c^n}{1 + k \times c^n} \qquad (10)$$

where, $\Delta R / R_0$ is the amount of NH_3 adsorbed by the sensor's surface (ppm), Q_{sat} is the maximum adsorption, k is a constant(kJ^2/mol^2) related to energy. In both cases, the sensor response behaviors showed good agreement with the Langmuir model. From this model, the saturation response of 1.35 and 1.33 was observed before and after bending mode measurements and the parameters are listed in Table I.

The sensor response time is the time required to cause a change in electrical resistance/conductance (R/C) on introducing NH_3 in a specific range by 90%. The calculated response time of the flexible CuO sensor lies between 5-9 min for different NH_3 concentrations. Fig. 6a shows the response and recovery kinetics of the fabricated sensor for different concentrations of NH_3 (5, 10, 20, 60 and 100 ppm).

It is worthy to mention that the sensor responded to 5 ppm of NH_3 in 90 s and recovered in 185 s. Fig.6b shows the variation of response and recovery items with respect to NH_3 concentration. It is seen that the response time decreases with increase in concentration while recovery time increases. In order to further analyze the A-D process of NH_3 on flexible CuO surface, the adsorption and desorption rate constants (τ) were estimated.

TABLE I
LANGMUIR ISOTHERM FITTING PARAMETERS OF FLEXIBLE CuO SENSING RESPONSE TOWARDS DIFFERENT CONCENTRATION OF NH_3

Mode	R^2	k	c	Q_{sat}
Flat mode	0.98	0.03	0.06	1.35
After bending	0.98	0.03	0.04	1.33

By considering the monolayer adsorption of reducing gas at T (Room Temperature), Langmuir adsorption kinetics for a single adsorption site with the conductance transient can be given as [34, 35],

$$C(t)_{resp} = C_0 + C_1[1 - \exp(-t/\tau_{resp})] \qquad (9)$$

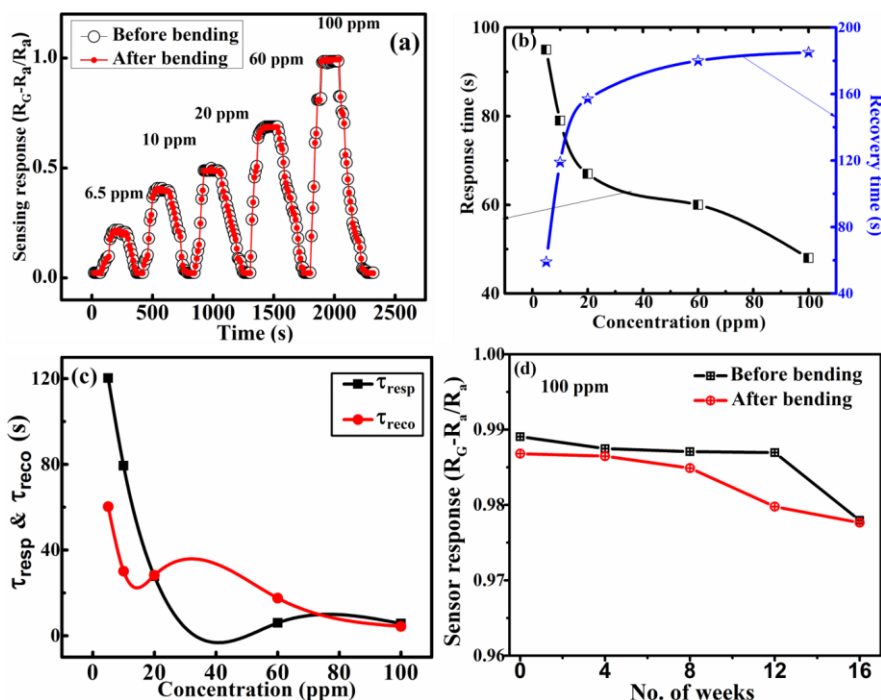$$C(t)_{rec}^* = C_0^* + C_1^*[-\exp(-t/\tau_{reco})] \qquad (10)$$

Fig.6. (a) Response - recovery plot of flexible CuO sensor for different concentrations of ammonia at Room Temperature, (b) variation of response and recovery times with ammonia concentration, (c) the time constant calculated from the regression analysis and (d) stability analysis of the sensor for 100 ppm of NH_3.

where, $[C(t)_{resp}]$ and $[C(t)_{rec}{}^*]$ are the conductance transients of response and recovery, respectively, C_0 and $C_0{}^*$ baseline conductance of the sensor and τ_{resp} & τ_{reco} are the relaxation times. The conductance corresponds to response of the flexible CuO sensor to different concentrations of NH_3 measured at room temperature is fitted according to the equation 9 and the results are presented in table. II (ESI† See supporting information Fig. S1). The R^2 values show that the fits are in good agreement. The non-significant change in the C_0 value suggests the negligible baseline drift with increase in gas concentration. Similarly, the conductance corresponding to recovery curve was also analyzed using desorption model in equation 10. The recovery plots of the flexible CuO sensor for different NH_3 concentrations are fitted well and the parameters obtained are also listed in Table II. Similar results were observed as response, the value of $C_0{}^*$ varied slightly which indicate the marginal baseline drift in the sensor. It can be observed that the metric of how rapid the NH_3 A-D process decreases as the gas concentration increases.

Fig.6c shows the plot of concentration vs. relaxation times. As seen in figure the linear relationship is maintained up to 20 ppm and it deviates from the linearity at around 60 ppm, from this aspect, it can be concluded that the response time with NH_3 concentration are likely governed by a physical process that involves the physi-adsorption of NH_3 on the CuO surface.

Stability of the flexible CuO sensor towards NH_3 gas was analyzed for 3 months with an interval of 21 days for 100 ppm of NH_3. From the Fig. 6d, it can be seen that there is no significant drift in the sensor response over a period of 2.5 months and a very slight drift afterwards can be observed. However, a decrease in response of about 0.07 % was observed which may be due to the humidity induced effect [38]. This long-term measurement reveals the good stability of the flexible CuO sensor. The observed sensing response of the flexible CuO sensor towards NH_3 at room temperature is comparable with the response observed for CuO thick films prepared on other substrates like glass slides [39].

TABLE II

ADSORPTION AND DESORPTION RATE PARAMETERS OBTAINED FROM THE FITTING OF TIME DEPENDENT CONDUCTANCE CHANGE IN THE PRESENCE AND ABSENCE OF AMMONIA.

C	Response transients			Recovery transients		
	τ_{resp}(s)	C_0 (10^{-7})	R^2	τ_{reco}(s)	$C_0{}^*$ (10^{-7})	R^2
6.5	120.25	40.14	0.98	60.28	2.15	0.98
10	79.36	39.55	0.99	30.12	0.80	0.98
20	8.75	40.35	0.99	28.23	0.92	0.97
60	6.02	40.12	0.98	22.56	1.92	0.99
100	5.7	40.21	0.98	4.36	2.81	0.98

TABLE III

COMPARISON OF SENSING PERFORMANCES

No	Material	Max. response/ NH_3 concentration	Ref
1	CuO Rods	0.98/1000	[40]
3	ZnO Rods	0.3/100	[41]
4	CuO Spheres, needles	0.8/100	[42]
5	rGO	0.8/100	[43]
7	CuO NRs	1/100	This work

Table III shows the comparison of sensing properties observed for different materials. It is interesting to reveal that the

fabricated flexible CuO sensor shows much better response at room temperature. Thus, the present investigation suggests that the fabricated flexible CuO sensor can selectively be used to detect low concentration of NH_3 at room temperature.

IV. CONCLUSION

CuO nanorectangles were successfully synthesized by a simple surfactant-free hydrothermal method. The X-ray diffraction analysis revealed the monoclinic phase of CuO with high crystallinity and purity. Flexible NH_3 sensor was fabricated by screen printing of CuO nanorectangle sample on flexible PET substrate. The sensor was able to respond to as low as 5 ppm to 100 ppm of NH_3 at room temperature. The highest response of 0.98 was achieved towards 100 ppm of NH_3. The response of the sensor at room temperature can be attributed to the large surface area available for gas adsorption to take place. The main advantage of the sensor is that it is operable at room temperature and does not require any external stimulus for response and recovery. Additionally, even after being subjected to bending deformation for 24 h, the sensor was able to reproduce the response with negligibly small drift. The stability measurements showed that the sensor response is not significantly affected by any humidity etc. over a period of 3 months. The overall superior performance of the sensor implies that it can be used in wearable and other hand-held sensor devices employed in diverse applications. As a future application, the sensor can be attached to cloths with low power electronics and the data will be transferred to mobile phones via radio frequency identification (RFID) methods.

References

[1]. M. Kampa, E. Castanas, "Human health effects of air pollution," *Environ. Pollut., Vol.* 151, pp. 362-367, 2008.

[2]. L. Horrigan, R.S. Lawrence, P. Walker, "How sustainable agriculture can address the environmental and human health harms of industrial agriculture," *Environ. Health Persp.,* Vol. 110, pp. 445-456, 2002.

[3]. L. Xu, S. Sithambaram, Y. Zhang, C.H. Chen, L. Jin, R. Joesten and S. L. Suib, "Novel urchin-like CuO synthesized by a facile reflux method with efficient olefin epoxidation catalytic performance," *Chem. Mater.*, Vol. 21, no. 7, pp. 1253-1259. 2009.

[4]. A. J. Bandodkar, I. Jeerapan and J. Wang, "Wearable chemical sensors: Present challenges and future prospects," *ACS Sensors*, Vol 1 no. 5, pp. 464-482, 2016.

[5]. N. Docquier and S. Candel, "Combustion Control and Sensors, A Review," *Progr. Energy Combust. Sci.* vol. 28, pp. 107–150, 2002.

[6]. C. S. Rout, M. Hegde, A. Govindaraj, C. N. R. Rao, "Ammonia sensors based on metal oxide nanostructures," Nanotech., Vol. 18, no. 20, pp. 205504, 2007.

[7]. S. Bhuvaneshwari and N. Gopalakrishnan, "Enhanced ammonia sensing characteristics of Cr doped CuO nanoboats," J. Alloys and Compd. Vol. 654, pp. 202-208, 2016.

[8]. P. Deka, R. C. Deka, P. Bharali, "Porous CuO nanostructure as a reusable catalyst for oxidative degradation of organic water pollutants," New J. Chem., Vol. 40, no. 1, pp. 348-357, 2016.

[9]. U. Altenberend, F. Molina-Lopez, A. Oprea, D. Briand, N. Bârsan, N. F. De Rooij, U. Weimar, "Towards fully printed capacitive gas sensors on flexible PET substrates based on Ag interdigitated transducers with increased stability," Sens. Actuators B Chem., Vol. 87, pp. 280-287, 2013.

[10]. Z. Q. Zheng, J. D. Yao, B. Wang, G. W. Yang, "Light-controlling, flexible and transparent ethanol gas sensor based on ZnO nanoparticles for wearable devices," Sci. rep., Vol. 5, pp.11070, 2015.

[11]. E. Comini, G. Faglia, G. Sberveglieri, Z. Pan and Z. L. Wang, "Stable and highly sensitive gas sensors based on semiconducting oxide nanobelts," Appl. Phy. Lett., Vol. 81, no. 10, pp. 1869-871, 2002.

[12]. Q. Wan, Q. H. Li, Y. J. Chen, T. H. Wang, X. L. He, J. P. Li, C. L. Lin, "Fabrication and ethanol sensing characteristics of ZnO nanowire gas sensors," Appl. Phy. Lett., Vol 84, no. 8, pp. 3654-3656, 2004

[13]. I. D. Kim, A. Rothschild, B. H. Lee, D. Y. Kim, S. M. Jo and H. L. Tuller, "Ultrasensitive chemiresistors based on electrospun TiO2 nanofibers," Nano Lett., Vol.6, no. 9, pp. 2009-2013, 2006.

[14]. H. G. Moon, Y. S. Shim, D. H. Kim, H. Y. Jeong, M. Jeong, J. Y. Jung and J. H. Lee, "Self-activated ultrahigh chemosensitivity of oxide thin film nanostructures for transparent sensors," Sci. rep., Vol. 2, pp. 588, 2012.

[15]. D. Zhang, Z. Liu, C. Li, T. Tang, X. Liu, S. Han and C. Zhou, "Detection of NO2 down to ppb levels using individual and multiple In2O3 nanowire devices," Nano let., Vol. 4, no. 10, pp. 1919-1924, 2004.

[16]. Y. H. Choi, D. H. Kim, S. H. Hong and K. S. Hong, "H2 and C2 H5 OH sensing characteristics of mesoporous p-type CuO films prepared via a novel precursor-based ink solution route," Sens. Actuators B Chem., Vol. 178, pp. 393-403, 2013.

[17]. Y. Liu, G. Zhu, B. Ge, H. Zhou, A. Yuan and X. Shen, "Concave Co3O4 octahedral mesocrystal: polymer-mediated synthesis and sensing properties," Cryst. Engg. Comm., Vol. 14, no. 19, pp. 6264-6270, 2012.

[18]. N. G. Cho, I. S. Hwang, H. G. Kim, J. H. Lee and I. D. Kim, "Gas sensing properties of p-type hollow NiO hemispheres prepared by polymeric colloidal templating method," Sens. Actuators B Chem., Vol. 155, no. 1, pp. 366-37, 201.

[19]. S. Xia, H. Zhu, H. Cai, J. Zhang, J. Yu and Z. A. Tang, Hydrothermally synthesized CuO based volatile organic compound gas sensor" RSC Adv., Vol. 4, no. 10, pp. 57975-57982, 2014.

[20]. Liao, L., Zhang, Z., Yan, B., Zheng, Z., Bao, Q. L., Wu, T., & Li, J. C. (2009). Multifunctional CuO nanowire devices: p-type field effect transistors and CO gas sensors. Nanotechnology, 20(8), 085203.

[21]. Yang, C., Su, X., Xiao, F., Jian, J., & Wang, J. (2011). Gas sensing properties of CuO nanorods synthesized by a microwave-assisted hydrothermal method. Sensors and Actuators B: Chemical, 158(1), 299-303.

[22]. Gou, X., Wang, G., Yang, J., Park, J., & Wexler, D. (2008). Chemical synthesis, characterization and gas sensing performance of copper oxide nanoribbons. Journal of Materials Chemistry, 18(9), 965-969.

[23]. Lee, J. H. (2009). Gas sensors using hierarchical and hollow oxide nanostructures: overview. Sensors and Actuators B: Chemical, 140(1), 319-336.

[24]. S. Khan, L. Lorenzelli and R. S. Dahiya, "Technologies for printing sensors and electronics over large flexible substrates: a review," IEEE Sens. J., Vol. 15, no. 6, pp. 3164-3185, 2015.

[25]. L. Manjakkal, B. Synkiewicz, K. Zaraska, K. Cvejin, J. Kulawik and D. Szwagierczak, "Development and characterization of miniaturized LTCC pH sensors with RuO2 based sensing electrodes," Sens. Actuators B Chem., Vol. 223, pp. 641-649, 2016.

[26]. Y. V. Kaneti, Z. Zhang, J. Yue, Q. M. Zakaria, C. Chen, X. Jiang and A. Yu, "Crystal plane-dependent gas-sensing properties of zinc oxide nanostructures: experimental and theoretical studies" Phys. Chem. Chem. Phys., Vol. 16, no. 23, pp. 11471-11480, 2014.

[27]. X. Gou, G. Wang, J. Yang, J. Park and D. Wexler, "Chemical synthesis, characterisation and gas sensing performance of copper oxide nanoribbons," J. Mater. Chem., Vol. 18, no. 9, pp. 965-969, 2008.

[28]. Debbichi, L., Marco de Lucas, M. C., Pierson, J. F., & Kruger, P. (2012). Vibrational properties of CuO and Cu4O3 from first-principles calculations, and Raman and infrared spectroscopy. The Journal of Physical Chemistry C, 116(18), 10232-10237.

[29]. Tiemann, M. (2007). Porous metal oxides as gas sensors. Chemistry-A European Journal, 13(30), 8376-8388.

[30]. B. Timmer, W. Olthuis and A. Van Den Berg, "Ammonia sensors and their applications—a review," Sens. Actuators B Chem., Vol. 107, no. 2, pp. 666-677, 2005.

[31]. C. Pijolat, C. Pupier, M. Sauvan, G. Tournier and R. Lalauze, "Gas detection for automotive pollution control," Sens. Actuators B Chem., Vol. 59, no. 2, pp. 195-202, 1999.

[32]. Koziej, D., Baˆrsan, N., Weimar, U., Szuber, J., Shimanoe, K., & Yamazoe, N. (2005). Water–oxygen interplay on tin dioxide surface: implication on gas sensing. Chemical Physics Letters, 410(4), 321-323.

[33]. Simion, C. E., Sackmann, A., Teodorescu, V. S., Ruşti, C. F., & Stănoiu, A. (2015). Room temperature ammonia sensing with barium strontium titanate under humid air background. Sensors and Actuators B: Chemical, 220, 1241-1246.

[34]. Hübner, M., Simion, C. E., Tomescu-Stănoiu, A., Pokhrel, S., Bârsan, N., & Weimar, U. (2011). Influence of humidity on CO sensing with p-type CuO thick film gas sensors. Sensors and Actuators B: Chemical, 153(2), 347-353.

[35]. Gurlo, A. (2006). Interplay between O2 and SnO2: oxygen ionosorption and spectroscopic evidence for adsorbed oxygen. ChemPhysChem, 7(10), 2041-2052.

[36]. G. Korotcenkov, "Handbook of gas sensor materials. Properties, Advantages and. Shortcomings for Applications Volume 1: Conventional Approaches. New York, USA: Springer. 2013.

[37]. J. U. Keller and R. Staudt, "Gas adsorption equilibria: experimental methods and adsorptive isotherms," Springer Science & Business Media, 2005.

[38]. K. Mukherje and S. B. Majumder, "Analyses of response and recovery kinetics of zinc ferrite as hydrogen gas sensor," J. Appl. Phys., Vol. 106, no. 6, pp. 06492, 2009.

[39]. A. N. Abbas, B. Liu, L. Chen, Y. Ma, S. Cong, N. Aroonyadet and C. Zhou, "Black phosphorus gas sensors," ACS nano., Vol. 9, no. 5, pp. 5618-5624, 2015.

[40]. Yang, Chao, Xintai Su, Feng Xiao, Jikang Jian, and Jide Wang. "Gas sensing properties of CuO nanorods synthesized by a microwave-assisted hydrothermal method." Sensors and Actuators B: Chemical 158, no. 1 (2011): 299-303.

[41]. Sun, Z. P., Liu, L., Zhang, L., & Jia, D. Z. (2006). Rapid synthesis of ZnO nano-rods by one-step, room-temperature, solid-state reaction and their gas-sensing properties. Nanotechnology, 17(9), 2266.

[42]. Singh, I. and Bedi, R.K., 2011. Surfactant-assisted synthesis, characterizations, and room temperature ammonia sensing mechanism of nanocrystalline CuO. Solid State Sciences, 13(11).

[43]. Barsan, N., C. Simion, T. Heine, S. Pokhrel, and U. Weimar. "Modeling of sensing and transduction for p-type semiconducting metal oxide based gas sensors." Journal of electroceramics 25, no. 1 (2010): 11-19.

Dr. Bhuvaneshwari Sakthivel is a doctoral student of Department of Physics, National Institute of Technology, Tiruchirappalli, India. She received her Bachelor's degree in Physics (2010) from PSG CAS, Bharathiyar University and Master's degree in Physics (2012) from National Institute of Technology, Tiruchirappalli, India. She completed her Ph.D in the field of metal oxide semiconductors for gas sensing applications National Institute of Technology, Tiruchirappalli, India..
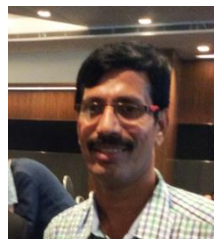
Dr. Gopalakrishnan Nammalvar received his B.Sc and M.Sc degrees in Physics from Madhurai Kamarajar University in 1988 and 1990 respectively. He obtained M.Phil degree and Ph.D. degree from Anna University, Chennai, India, in 1991 and 1997, respectively. He is currently working as a Associate Professor at the Department of Physics, National Institute of Technology, Tiruchirappalli, India. He was with universities in Sweden (KTH), Japan (AIST) and South Korea (DEU) as a Post-Doctoral Researcher. His current research interests include the growth of III-V and II-VI semiconductor thin films and nanostructures for optoelectronics, spintronics and gas sensing applications. He was a recipient of the prestigious STA Fellowship offered by Japan Science and Technology (JST) Association for Crystal Growth. He is life member at Indian Association for Crystal Growth (IACG), the Magnetic Society of India and the Indian Society for Non-Descriptive Technique (ISNT).

Dr. Libu Manjakkal received B.Sc. in Physics from Calicut University, India in 2006, M.Sc. in Physics from Mahatma Gandhi University, Kerala, India in 2008 and Ph.D. in electronics with honors from Institute of Electron Technology (ITE), Warsaw, Poland, in 2015. His Ph.D. thesis was related to metal oxide based thick film pH sensors. In the period 2009–2012 he was involved in two research and development projects at C-MET, Thrissur, Kerala, India. He also worked in CEMOP/UNINOVA, New University of Lisbon, Portugal for the period May–July 2012. From 2009 to 2012 he was involved in two research and development projects at the Center for Materials for Electronics Technology, Thrissur, India. In 2012, he was with CEMOP/UNINOVA, New University of Lisbon, Portugal. From 2012 to 2015, he was as an Early Stage Researcher Fellow in the framework of Marie Curie ITN Program within the SENSEIVER Project, ITE. From 2015 to 2016, he was a Post-Doctoral Researcher with ITE. From June 2016 to September 2016, he was a Marie Curie experienced researcher at BEST Group, Electronics and Nanoscale Engineering Research Division, University of Glasgow, U.K, and currently working as a Post-Doctoral Fellow in the same Institute within the EPSRC Project PRINTSKIN. He has authored or co-authored 28 scientific papers. His current research interests comprise flexible and printable electronics, supercapacitors, electrochemical sensors, LTCC technology, multilayer actuators, TCO films, pH sensors, and gas sensors.